

Tune without Validation: Searching for Learning Rate and Weight Decay on Training Sets

Lorenzo Brigato and Stavroula Mougiakakou

ARTORG, University of Bern, Switzerland
{name}. {lastname}@unibe.ch

Abstract. We introduce **Tune without Validation** (Twin), a pipeline for tuning learning rate and weight decay without validation sets. We leverage a recent theoretical framework concerning learning phases in hypothesis space to devise a heuristic that predicts what hyper-parameter (HP) combinations yield better generalization. Twin performs a grid search of trials according to an early-/non-early-stopping scheduler and then segments the region that provides the best results in terms of training loss. Among these trials, the weight norm strongly correlates with predicting generalization. To assess the effectiveness of Twin, we run extensive experiments on 20 image classification datasets and train several families of deep networks, including convolutional, transformer, and feed-forward models. We demonstrate proper HP selection when training from scratch and fine-tuning, emphasizing small-sample scenarios.

1 Introduction

Like most machine learning models, deep networks are configured by a set of hyper-parameters (HPs) whose values must be carefully chosen and which often considerably impact the final outcome [17, 26, 60]. Setting up wrong configurations translates into bad performance, particularly in the most difficult optimization scenarios, e.g., large models that overfit on small datasets [4, 5, 35].

Traditionally, HP search is performed in two ways, as exemplified in Fig. 1 (top). Although more comprehensive methodologies, such as multi-fold or multi-round cross-validation [44], exist, they are scarcely employed in training deep networks due to their significant computational overhead. When no validation set is available, the training set is split into two unbalanced subsets to perform the HP search. Then, the “optimal” HP configuration initializes the final training on the original collection. In contrast, if the validation set is accessible, ML professionals can expedite the HP search and simplify the model selection process since the two-step training pipeline is avoided. However, this comes at the expense of collecting an additional 10-30% of samples. Use cases where acquiring additional data is either expensive or logistically unfeasible, such as medical imaging [50] or federated learning [37], challenge the traditional HP selection pipeline. HP optimization on small validation sets may have inherent noise [7, 35].

Motivated by these challenges, we introduce **Tune without Validation** (Twin), an innovative HP selection approach inspired by a theoretical framework which

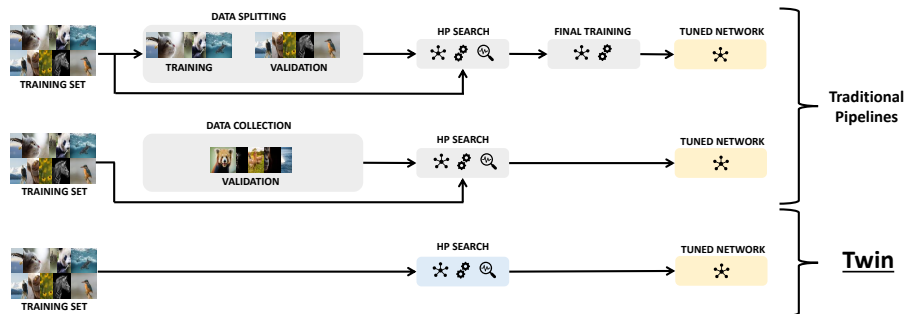


Fig. 1: Overview. While traditional pipelines need a validation set to tune learning rate and weight decay, Twin performs the search directly on the training set, simplifying the process or saving additional data-collection costs.

aims at explaining representation learning across HPs from phase diagrams [33]. Twin obviates the need for validation sets when tuning optimizer parameters. In particular, Twin enables practitioners to directly select the learning rate (LR) and weight decay (WD) from the training set, as sketched in Fig. 1 (bottom). Twin performs a grid search over an hypothesis space using an early-/non-early-stopping scheduler and successfully predicts generalizing HP configurations by monitoring only the training loss, as a proxy for task performance, and the weight norm, to measure regularization strength.

We perform an extensive empirical analysis to demonstrate Twin’s practical versatility by training 4,000+ deep models involving 20 datasets and several architectures. On a suite of 34 different dataset-architecture configurations with networks trained from scratch and without early stopping, Twin scores an MAE of 1.3% against an *Oracle* pipeline - the ideal unrealistic scenario - that directly selects HPs from testing sets. We summarize the contributions of our paper:

- We introduce Twin, a simple but effective HP selection pipeline which optimizes LR and WD, directly from training sets (Sec. 3).
- We showcase the effectiveness of Twin across a wide spectrum of experimental scenarios (Sec. 4.1, Sec. 4.2, Sec. 4.3, Sec. 4.4), encompassing datasets from different domains (e.g., natural, medical imagery) and scales (hundreds to thousands of samples) as well as models with various architecture (e.g., ResNet, MLP, CVT) and size (from $\sim 0.2\text{M}$ to $\sim 90\text{M}$ params.).
- We ablate on the different components and parameters of Twin to provide additional insights regarding the working mechanisms of our pipeline (Sec. 4.5).

2 Related Work

Image classification. Since the introduction of AlexNet [26], image classification has witnessed remarkable advances, propelled by the development of

novel neural architectures (e.g., ResNet [16], Vision Transformer (ViT) [11]), and large datasets [42]. Large-scale pre-training has favored the application of transfer learning to tackle small-sample scenarios [24,54]. More recent work provides insights regarding the training of deep models from scratch on limited datasets [1,5,6,8,28,56]. Motivated by the medium-to-small size of datasets explored in this work, we mostly train convolutional networks (ConvNets) but also experiment with ViTs and feed-forward networks.

Hyper-parameter tuning. There is a vast literature tackling the problem of HP tuning for deep networks [60], including works on implicit differentiation [35], data augmentation [10,31], neural-architecture search [12], invariance learning [3,21,55], and general-purpose schedulers [29,30]. Concerning optimization-related HPs, the seminal work of Goyal et al. [14] popularized the linear scaling rule for learning rate and batch size. Yang et al., [58] proposed a parameterization to zero-shot transfer LRs to larger model sizes [58]. Recent work studied HP selection as data scales by exploiting SGD symmetries [61,62]. However, only a few studies explore HP optimization without employing validation sets, mainly focusing on learning invariances. When employing Bayesian inference, methods either fail to scale to relatively simple tasks (e.g., CIFAR-10) [43] or larger network sizes (e.g., ResNet-14) [21]. Benton et al. [3] make strong assumptions about knowing what HPs help learning invariances in advance. A recent method improves scalability issues but still introduces complexity by needing data and model partitioning and an additional backward-forward pass [38]. Unlike such methods, Twin focuses on LR and WD, easily scales to increased model and data sizes, and simplifies the HP optimization pipeline.

3 Tune without Validation

3.1 Preliminaries

Problem settings. Image classification tasks present a training set $\mathcal{D}_{train} = \{x_i, y_i\}$ and a testing set $\mathcal{D}_{test} = \{x_i, y_i\}$ sampled from a distribution $P(X, Y)$. The learners, in our case, deep neural networks f_θ parameterized by parameters θ , are trained via SGD optimization to minimize the cross-entropy loss over the training set, $\min_\theta(\mathcal{L}_\theta = \mathcal{L}(f_\theta, \mathcal{D}_{train}))$. A popular regularization technique to avoid over-fitting and improve generalization is L_2 regularization, i.e., $\min_\theta \hat{\mathcal{L}}_\theta$ with $\hat{\mathcal{L}}_\theta = \mathcal{L}(f_\theta, \mathcal{D}_{train}) + \lambda \cdot \frac{\|\theta\|^2}{2}$ that features a penalty over the norm of the weights controlled by the parameter λ , widely known as WD. For modern scale-invariant architectures¹, WD does not reduce the complexity of the model but rather increases the *effective learning rate* by reducing the weight norm [48,64], and hence can indirectly exert a regularizing effect by means of larger gradient noise [22,32,39]. When optimized with momentum SGD, the parameters follow the update rule $\theta_{t+1} = \theta_t - \mu v_t + \alpha_t(\nabla \mathcal{L}_\theta + \lambda \theta_t)$ where α_t being the LR adjusted at each iteration according to a LR schedule and μ the momentum coefficient.

¹ Up to 90% of the parameters in ResNets tend to be scale-invariant, primarily due to the influence of Batch Normalization [20].

Cross-validation. To estimate the HPs controlling the model, specifically the regularization parameter λ and the learning speed α , we ideally need a surrogate of the test set, which identifies the right model complexity that minimizes the test error. As anticipated previously, the simplest (and most popular) operation is to split the training set into two sub-datasets to deliver a smaller training set and a validation set $\mathcal{D}_{val} = \{x_i, y_i\}$, as shown in Fig. 1 (top). The cardinality of the sub-sampled training and validation sets are respectively $|\hat{\mathcal{D}}_{train}| = n - m$ and $|\hat{\mathcal{D}}_{val}| = m$. Now, we define the expected value and variance of the prediction error over unseen points respectively as $\delta = \mathbb{E}[\mathcal{L}(f_\theta(x), y)]$ and $\sigma^2 = \text{Var}[\mathcal{L}(f_\theta(x), y)]$. We also refer to the loss computed over the validation set as $\mathcal{L}(f_\theta, \mathcal{D}_{val}) = \sum_{i=1}^m \mathcal{L}(f_\theta(x_i), y_i)$. By applying the linearity property of the expectation and the previously defined relationships, we derive that $\mathbb{E}[\mathcal{L}(f_\theta, \mathcal{D}_{val})] = \delta$, $\text{Var}[\mathcal{L}(f_\theta, \mathcal{D}_{val})] = \frac{\sigma^2}{m}$, and $\text{Std} = \mathcal{O}(\frac{1}{\sqrt{m}})$. Finally, we can express that the expected error on the validation set is proportional to the error scored over an unseen test sample plus a term depending on the number of samples in the validation split, or more formally $\mathbb{E}[\mathcal{L}(f_\theta, \mathcal{D}_{val})] = \delta \pm \mathcal{O}(\frac{1}{\sqrt{m}})$. The straightforward consequence is that a small validation set does not provide a good estimate of the test error; hence, it is unreliable for HP selection.

Motivation. In classification problems where the *independent and identically distributed* (IID) assumption holds, the search for HPs is less challenging since the overlapping among training and testing sets makes the prediction of generalization relatively easy. In other words, if \mathcal{D}_{train} , and \mathcal{D}_{test} are sampled from the same distribution, the expected prediction error δ on unseen test points is going to be proportional to the prediction error over the training set, i.e., $\delta \approx \mathcal{L}(f_\theta, \mathcal{D}_{train})$. In section Sec. 4.1, we further discuss this claim and indeed empirically validate it in Fig. 3. On the contrary, distribution shifts, possibly caused by a plethora of factors such as corruptions [19] or lack of data [52], induce the so-called *out-of-distribution* (OOD) learning problems. In this work, we focus on OOD scenarios caused by sample scarcity. As demonstrated in the previous paragraph, the number of samples available in the validation set strongly impacts the expected prediction error and can bias the search for proper HPs. The significance of this observation is the main motivation guiding our work, which aims to eliminate the dependency on validation sets and make the search for LR and WD more robust. Our paper aims to derive a robust recipe for practically predicting HP generalization in IID and OOD settings.

3.2 Working Principle

Phases of learning. We rely on a recently introduced theoretical framework that explains representation learning and the recently observed behavior of *grokking* [41], a phenomenon where models generalize long after overfitting their training set. Precisely, Liu et al. [33] observe, via a macroscopic analysis of phase diagrams describing learning performance across HPs, four learning phases: i) *comprehension*, ii) *grokking*, iii) *memorization*, and iv) *confusion*. The last two

phases correspond to the well-known overfitting and underfitting scenarios, while *comprehension* to standard representation learning and *grokking* to delayed generalization.² We leverage the following observations to design Twin [33]:

- Observation 1 (O1): The *comprehension*, *grokking*, and *memorization* phases all share the learner to reach a low enough training error.
- Observation 2 (O2): Out of the three phases of O1, only the *comprehension* and *grokking* configurations manage to reach a low-enough testing error.
- Observation 3 (O3): Representation learning (*comprehension* and *grokking*) occurs only in a “Goldilocks zone” between *memorization* and *confusion*.

Intuition. Our goal is to predict generalizing configurations of LR and WD from a defined hypothesis space. Configurations that lie in the *comprehension* or *grokking* areas provide the best generalization performance. However, the definitions to classify learning phases, as proposed in [33], leverage validation error, a metric that we are willing to avoid. According to O1, low training error excludes the phase with *confusion* (underfitting). Monitoring the training loss can hence identify configurations that underfit the training objectives. However, O2 predicts that only *comprehension* and *grokking* reach low testing errors. Reasonably, the training loss alone can not discern overfitting from generalizing solutions. To identify *memorization* within the hypothesis space, we leverage O3 and recognize that the norm of the network’s parameters provides a suitable metric for assessing the transition from *confusion* to *memorization*, passing through *comprehension*. High WD strongly penalizes the parameter’s norm, leading to *confusion*, while low WD causes *memorization* since the model is poorly regularized. In summary, we employ the training loss as a proxy to identify underfitting configurations. Out of the remaining models, we expect the generalizing configurations to be the ones with the lowest norm of the parameters. Fig. 4 strongly supports our hypothesis and shows the predictive power of the parameter norm related to model generalization. We next describe Twin’s pipeline in practice.

3.3 Pipeline

We show the overview of Twin in Fig. 2. Twin performs a grid search over the LR-WD space and optimizes deep networks via gradient-based methods. Trials are scheduled according to a first-input-first-output scheduler (no early-stopping) or successive-halving-based scheduler that reduces the computational burden. Then, a simple cascade of segmentation and filtering modules identifies the training loss region where generalization or overfitting happens. Within this area, the network with the smallest parameter norm is selected.

Grid search and trial scheduler. Twin runs $N_\alpha \cdot N_\lambda$ trials sampled by default from a grid of equally spaced points in logarithmic space for both LR and WD. However, Twin also supports different grid densities as ablated in Sec. 4.5.

² Note that *grokking* is mostly observed in algorithmic tasks, but can also be induced for image classification problems [33, 34]

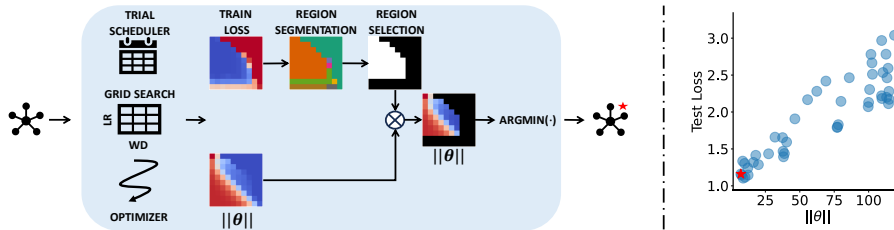


Fig. 2: Twin overview. Twin employs a gradient-based optimizer and a trial scheduler to perform a grid search across the LR-WD space. Twin logs train-loss and parameter-norm matrices to identify the network with the lowest norm within the fitting region. The parameter norm within this region is a good predictor of generalization (right plot). In this figure, we show as an example a WRN-16-10 trained on ciFAIR-10.

We experiment with two types of trial schedulers: 1) a default first-input-first-output (FIFO) without any form of automated trial stopping and 2) HyperBand (HB) [30]. Other trial schedulers (e.g., median stopping rule [13]) and search strategies (e.g., random search) are left for future exploration. Default HP search over validation sets usually terminates a few HP configurations, out of which the optimal is picked. Conversely, as anticipated in Sec. 3.2, Twin needs to detect the region in the LR-WD space with low training loss. Trial stopping too aggressively would make the loss landscape noisy and challenging to segment. To this end, we adapted the HB scheduler to our needs. More precisely, we run the original HB algorithm until only a certain percentage X of trials is still alive and continue such trials without further stopping. In other words, we systematically pass the most promising trials to the bottom rung. The asynchronous version of HB, Asynchronous Successive Halving Algorithm (ASHA) [29], employs a similar mechanism to exploit parallelism. We opt for this solution rather than increasing the minimum resources per trial to save compute resources. We refer to our adapted HB with $\text{HB}_{X\%}$ when $X\%$ of the trials are terminated. In Sec. 4.5, we ablate on the impact of different levels of early stopping, i.e., $X\% \in \{25\%, 12\%\}$, and show that Twin supports aggressive stopping well.

Region segmentation and selection. The grid search guided by the trial scheduler yields two log matrices needed to find the optimal configuration: training losses and parameter norms. We refer to the first matrix as Ψ and the second as Θ . Note that the matrix elements are logged at different epochs when early stopping is employed. In the case of the training losses, we average the values of the last five training epochs to have a more reliable estimate. To identify the area of the LR-WD space where the best fitting happens, we treat the loss matrix as an image and apply the popular Quickshift image segmentation algorithm [51]. Quickshift proved to be more robust than hand-crafted thresholds that fail to generalize across diverse datasets and model configurations. Quickshift needs two input parameters, namely `kernel_size` and `max_dist`, which control the segmentation granularity. We set both parameters to the squared root of the

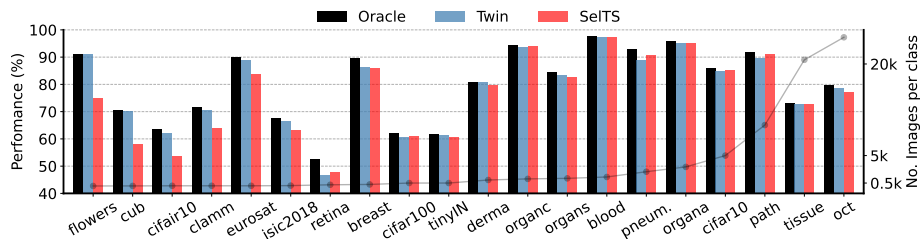


Fig. 3: Overview of quantitative results. Twin scores an overall 1.3% MAE against the *Oracle* pipeline across 34 different dataset-model configurations when using a FIFO scheduler. Twin closely matches the *Oracle* in IID and OOD scenarios, while SelTS fails to correctly predict HPs that generalize in OOD cases.

largest grid side to have a more fine-grained segmentation. We ablate on this choice in Sec. 4.5. Practically, we first filter possible outliers, e.g., exorbitant loss values or NaN, stemming from instabilities during training caused by extreme parameter configurations. We consider outliers all points having a *z-score* larger than two. We then scale the values of Ψ to 0-1 range by *minmax* normalization, make the lowest loss the highest value ($|1 - \text{minmax}(\Psi)|$), and run *Quickshift* segmentation. We finally take the mean for each predicted region and apply the *argmax* to retrieve the best cluster index.

Output configuration. The selected grid region is converted into a binary mask and applied to the logged Θ matrix. Out of this sub-region, the *argmin* function returns the final output configuration with the lowest norm.

4 Experiments

4.1 Overview

Experimented domains. In selecting datasets for experimentation, we aimed to cover diverse domains to thoroughly assess Twin’s capabilities. Firstly, our evaluation encompasses small datasets, a scenario particularly suitable for Twin, given that traditional pipelines struggle with HP selection due to the limited dimensions of validation sets, as explained in the paragraph dedicated to cross-validation of Sec. 3.1. Additionally, we explore Twin’s potential in the medical field, where its ability to mitigate the need for validation sets is particularly valuable, considering the complexities and regulations inherent in healthcare settings. Finally, we examine Twin’s versatility in dealing with natural images, arguably the most widely studied domain within the computer vision community.

Baselines. To assess the relative effectiveness of Twin, we introduce three different baselines. The *Selection from Training Set* (SelTS) baseline selects the

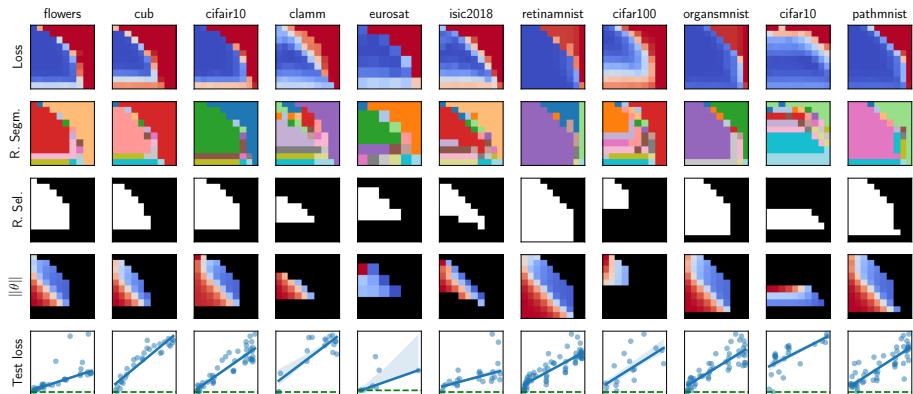


Fig. 4: Qualitative results. Visualization of the various steps of Twin in the LR-WD space (first four rows) and the relationship between the selected parameter norms and test loss (bottom row). The dashed green line represents the lowest achievable test loss.

HP configuration, which scores the lowest loss on the training set. The *Selection from Validation Set* (SelVS) is the more traditional reference point, where HP optimization is conducted exclusively on the validation set. The validation set can either be subsampled from the training set, as is going to be the case for small and natural image datasets, or collected externally, like the case of medical data. These two cases indeed correspond to the upper two schemes of Fig. 1. SelVS can also be performed with different trial schedulers, e.g., with early stopping. Lastly, the *Oracle* represents the ideal but unrealistic scenario of selecting HPs directly from the test set. The *Oracle* always runs a FIFO scheduler. When Twin performs at its absolute best, it yields an MAE of 0% vs the *Oracle*. All baselines select the HPs according to the relevant last-epoch metric with FIFO schedulers and the average of the last 5 with early stopping.

Quantitative results. To provide an overview of the quantitative results, we compare Twin against our lower (SelTS) and upper (*Oracle*) bounds in Fig. 3. In particular, we show the performance per dataset with FIFO schedulers averaged across all architectures. The order along the x-axis represents the number of images per class per dataset, which increases from left to right. As anticipated in Sec. 3.1, the training loss alone as an HP-selection metric (SelTS) falls short as the alignment between training and testing distributions decreases, i.e., when the IID assumption does not hold because the training set does not fully represent the broader testing set [49, 52]. On the other hand, we find nearly optimal LR-WD configurations across all dataset scales by considering the regularization strength and the task-learning performance, as done with Twin (Sec. 3.2).

Qualitative results. In Fig. 4, we present qualitative results and empirical evidence supporting Twin’s ability to predict generalizing HP configurations.

Method	Model	CUB	ISIC 2018	EuroSAT	CLaMM	Average
<i>Oracle</i>	EN-B0	67.2	66.8	91.0	65.3	72.6
SelTS	EN-B0	62.4	64.0	79.8	56.8	65.8
SelVS	EN-B0	67.0	65.1	86.6	58.0	69.2
<u>Twin</u>	EN-B0	66.2	66.4	89.8	62.6	71.3
<i>Oracle</i>	RN50	72.0	69.4	90.2	74.6	76.6
SelTS	RN50	57.3	65.4	83.8	68.2	68.7
SelVS [†]	RN50	70.8	64.5	90.6	70.2	74.0
<u>Twin</u>	RN50	70.1	68.8	89.2	73.8	75.5
<i>Oracle</i>	RNX101	73.0	66.7	88.6	75.2	75.9
SelTS	RNX101	54.2	59.8	86.8	62.5	65.8
SelVS	RNX101	72.1	62.4	90.0	70.1	73.7
<u>Twin</u>	RNX101	73.0	65.8	87.6	75.2	75.4

Table 1: Small datasets. The evaluation metric is the balanced test accuracy (%) [5]. We allocate 100 and 36 trials for EN-B0/RN50 and RNX101, respectively. Twin and SelVS respectively employ the HB_{25%} and ASHA schedulers. [†]Values are taken from [5].

We demonstrate Twin’s consistency across 11 cases involving different models (ConvNets, MLPs, and transformers), optimizers (SGD, Adam), and grid densities (100 and 49 trials). In Fig. 4, the first row displays the training loss at the last epoch. Region segmentation and selection steps using Quickshift are shown in the second and third rows, respectively. The fourth row illustrates the mask application to the parameter norm matrix, while the last row depicts the relationship between the parameter norm of the selected sub-region and the test loss. The dashed green line represents the lowest loss achieved by the *Oracle* baseline. Indeed, despite the best-fitting region showcasing various patterns and positions in the LR-WD space depending on the dataset-architecture configuration, Twin can identify it robustly. Furthermore, it is visible that a strong (almost linear) relationship exists between the parameter norms extracted from the identified region and the test loss.

4.2 Small Datasets

Datasets. We select the benchmark introduced in [5], which contains five different datasets spanning various domains and data types. In particular, the benchmark contains sub-sampled versions of ciFAIR-10 [2], EuroSAT [18], CLaMM [45], all with 50 samples per class, and ISIC 2018, with 80 samples per class [9]. Also, the widely known CUB dataset with 30 images per category is included [53]. The spanned image domains of this benchmark hence include RGB natural images (ciFAIR-10, CUB), multi-spectral satellite data (EuroSAT), RGB skin medical imagery (ISIC 2018), and grayscale hand-written documents (CLaMM). For EuroSAT, an RGB version is also available. Finally, we include the Oxford Flowers dataset in our setup, which comprises 102 categories with 20 images [40].

Implementation details. Along with the popular ResNet-50 (RN50), which was originally evaluated on the benchmark [5], we also employ EfficientNet-B0 (EN-B0) [46] and ResNeXt-101 (32 × 8d) (RNX101) [57] to cover three classes

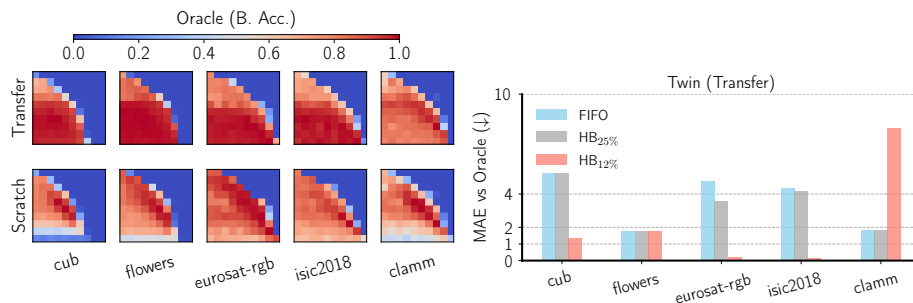


Fig. 5: Transfer learning. (Left) Normalized balanced accuracy of the *Oracle* with ImageNet pre-trained (top) or from-scratch RN50 (bottom). Feature overlap makes the best generalization appear with lower regularization, and Twin (with EN-B0, RN50, RNX101) plus early stopping identifies this region by scoring a low MAE (right).

of model scales, respectively *tiny*, *small*, and *base* [47], with 5.3M, 25.6M, and 88.8M parameters. For the low-resolution images of ciFAIR-10, we employ a Wide ResNet 16-10 (WRN-16-10). We refer the reader to the Appendix for all the details regarding training-related parameters. We perform squared grid searches of 100 trials for RN50 and EN-B0 and 36 trials for RNX101. We set the LR and WD intervals for the grid search to $[5 \cdot 10^{-5}, 5 \cdot 10^{-1}]$ to span four orders of magnitude. When training from scratch, we report results for Twin and SelVS with early stopping, which respectively employ HB_{25%} and ASHA as schedulers, with the same number of trials. For the parameters, we follow [5] and keep a halving rate of two and a grace period of 5% of the total epoch budget.

Results from scratch. As visible in Tab. 1, Twin nearly matches the *Oracle* balanced accuracy by scoring an MAE of less than 1.5% across different datasets and networks. Twin outperforms the traditional HP selection from the validation sets (SelVS) by scoring 71.3% versus 69.2% with EN-B0, 75.5% vs 74% with RN50, and 75.4 vs 73.7 with RNX101 when averaging performance across the CUB, ISIC 2018, EuroSAT, and CLaMM datasets. Indeed, SelVS relies on a small validation set, which may lead to sub-optimal HPs given the higher variability of the prediction error. Furthermore, despite aggressive trial stopping making the optimal region-segmentation step more challenging, Twin still finds semi-optimal LR-WD configurations and hence is scalable to computationally heavy search tasks that would be prohibitive without early stopping strategies.

Results with transfer learning. When dealing with small datasets, it is common practice to start from a network pre-trained on a larger amount of data (e.g., ImageNet [42]). Therefore, we also experiment with transfer learning and repeat the optimization runs with checkpoints initialized from ImageNet. In Fig. 5 (left), we notice that the generalization of networks as a function of the LR-WD space may differ from when training from scratch, and the main cause regards the

Method	Path	Derma	OCT	Pneum.	Retina	Breast	Blood	Tissue	OrganA	OrganC	OrganS	Avg.
<i>Oracle</i>	91.9	80.8	79.8	92.8	52.5	89.7	97.8	73.2	95.9	94.5	84.4	84.8
SelTS	91.9	79.7	77.3	90.7	47.8	85.9	97.2	72.8	95.0	94.0	82.8	83.2
SelVS	90.5	80.3	78.0	92.5	46.0	85.3	96.9	72.8	94.9	94.4	83.5	83.2
<u>Twin</u>	88.5	80.8	78.6	88.9	46.7	86.5	97.3	72.7	95.3	93.7	83.4	82.9

Table 2: Medical images. The performance is the test accuracy (%). We allocate a 100-trial budget per dataset. Both Twin and SelVS employ the FIFO scheduler.

overlapping between the source and target domains. Expectedly, with a strong class (CUB and Flowers) or feature (EuroSAT RGB, ISIC 2018) overlap, the best *comprehension* region shifts towards smaller regularization. To this end, Twin struggles, as visible from the higher MAE ($\sim 5\%$) in the cases of CUB, EuroSAT RGB, and ISIC 2018. As a solutions, we employ early stopping to terminate the mostly regularized trials whose training loss has a slower decay rate. In Fig. 5 (right), it is indeed visible that Twin with $HB_{12\%}$ reduces the MAE vs the *Oracle* to $\leq 1\%$ for CUB, EuroSAT RGB, and ISIC 2018. Conversely, in the case of CLaMM, which has no class and poor feature overlap (hand-written documents), the pre-trained checkpoints do not alter the LR-WD landscape and enable Twin to find good HP configurations ($< 2\%$ MAE) with the FIFO and $HB_{25\%}$ schedulers. In summary, when applying transfer learning, it is critical to consider the level of domain overlap to select the more suitable Twin configuration.

4.3 Medical Images

Datasets. We leverage the MedMNIST v2 benchmark [59] to test Twin on medical imaging tasks. We focus on 2D classification and select 11 out of 12 binary/multi-class or ordinal regression tasks of the MedMNIST2D sub-collection, which covers primary data modalities (e.g., X-ray, OCT, Ultrasound, CT, Electron Microscope) and data scales (from 800 to 100,000 samples). The MedMNIST2D benchmark provides held-out validation sets to allow HP tuning. The data diversity of this benchmark presents a significant challenge. We select the testbed with the images pre-processed to 28×28 resolution out of the full benchmark to maintain the total computational load under a reasonable budget.

Implementation details. We use the ResNet-18 (RN18) originally employed in the benchmark [59], which consists of four stages, as the version developed for ImageNet classification [16], but with a modified stem more suitable for low-resolution images. We keep the same Twin configurations tested on small datasets (Sec. 4.2), except for the trial schedulers that we default to FIFO for both Twin and SelVS. Refer to the Appendix for additional details on the implementation.

Results. We summarize the empirical results over MedMNIST2D in Tab. 2. The *Oracle* scores an upper bound 84.8% test accuracy averaged across the 11 tasks. Twin is comparable to the traditional SelVS (82.9% vs 83.2%). Note also

Dataset	Model	# Trials	Aug.	<i>Oracle</i>	SelTS	SelVS	<u>Twin</u>
C10	MLP-4-256	100	+	66.1	65.1	65.9	65.4
C10	CCT-2/3×2	49	+++	87.3	87.3	87.3	86.7
C10	RNX11	100	+	90.7	90.2	90.6	89.8
C10	RN20	100	+	92.7	91.8	92.4	90.5
C10	WRN-40-2	49	++	94.0	93.7	93.3	93.6
C100	MLP-4-512	100	++	35.4	35.0	35.1	34.9
C100	CCT-2/3×2	49	+++	65.0	64.0	65.0	65.0
C100	RNX11	100	+	68.8	67.7	68.6	66.8
C100	RN20	100	+	69.8	67.6	69.0	68.2
C100	WRN-40-2	49	++	74.2	74.2	72.8	72.8
TinyIN	CVT-7/8	36	+++	58.0	58.0	58.0	58.0
TinyIN	WRN-16-4	49	++	61.8	60.8	61.8	61.3
Average				72.0	71.3	71.6	71.1

Table 3: Natural Images. The performance is reported in test accuracy (%). FIFO scheduler is employed. For the strength of data augmentation, refer to the Appendix.

that Twin slightly improves its performance in this domain when early stopping is employed (Sec. 4.5). Twin finds proper HPs and simultaneously leads to a cost-effective solution by reducing data collection and labeling expenses associated with the $\sim 10\%$ of samples per dataset originally allocated for validation.

4.4 Natural Images

Datasets. Finally, we test Twin on popular natural-image datasets such as CIFAR-10/100 [25] and Tiny Imagenet [27]. These datasets contain 50,000/100,000 training samples from 10 to 200 classes, with an image resolution of 32×32 for CIFAR and 64×64 for TinyImagenet.

Implementation details. For CIFAR datasets, we employ ConvNets, transformers, and feed-forward networks. As ConvNets, we select ResNet-20 (RN20) [16], ResNeXt-11 ($4 \times 16d$) (RNX11) [57], and a Wide ResNet of depth 40 and width two (WRN-40-2) [63]. As transformers, we train architectures specifically designed for CIFAR, such as the Compact Convolutional Transformer with two encoder and convolutional-stem layers (CCT-2/3×2) [15]. We employ a Multi-Layer Perceptron (MLP) with batch normalization, ReLU activations, and hidden layers of constant width as feed-forward networks. We set the depth of the MLP to four layers and the width to 256 units for CIFAR-10 and 512 units for CIFAR-100 (MLP-4-256 and MLP-4-512). On TinyImagenet, we train a WRN-16-4 [63] and a Compact Vision Transformer [15] with seven encoder layers and a patch size of 8 (CVT-7/8). We vary the data augmentation strength from base to medium to strong $\{+, ++, +++\}$. Refer to the Appendix for additional details.

Results. As shown in Tab. 3, Twin is, on average, comparable to SelVS (71.1% vs 71.6%), despite not having access to the validation set, and SelTS (71.1% vs 71.3%), while considering the regularization strength along with the training loss.

kernel_size	max_dist	MAE	α			λ			MAE
			[::1]	:::2]	:::3]	[::1]	:::2]	:::3]	
N_α	N_α	9.4	✓			✓			1.3
$\sqrt{N_\alpha}$	N_α	4.2	✓				✓		1.4
N_α	$\sqrt{N_\alpha}$	1.4		✓		✓			1.8
N_α	$\sqrt{N_\alpha}$	1.4		✓			✓		1.5
$\sqrt{N_\alpha}$	$\sqrt{N_\alpha}$	1.3	✓					✓	1.5
					✓	✓			1.2
					✓			✓	1.2

(a) Quickshift

(b) Grid density

Table 4: Ablation studies concerning: (a) Quickshift controlling the segmentation density and (b) the robustness of Twin against the grid density. The MAE (\downarrow) is computed against the *Oracle* baseline.

Scheduler	Small Datasets			Medical Datasets
	EN-B0	RN50	RNX101	RN18
FIFO	71.3	75.2	75.4	82.9
HB _{25%}	71.3	75.5	75.4	83.8
HB _{12%}	71.5	74.9	69.8	83.2

Table 5: Ablation on early stopping for Twin. The performance is the average balanced test accuracy (%) on small datasets and test accuracy (%) on medical datasets.

Remarkably, we also notice that Twin works properly for transformers and MLPs, confirming that the intuition behind Twin translates well to various network architectures. Similarly, Twin is agnostic to the data-augmentation strength.

4.5 Ablations

Quickshift. We ablate on the impact of `kernel_size` and `max_dist` from Quickshift in Tab. 4a. In this analysis, we assume a squared grid ($N_\alpha = N_\lambda$) and hence report the parameters as a function of N_α only. We consider $\max(N_\alpha, N_\lambda)$ when the grid is not squared. In Tab. 4a, it is visible that setting `max_dist` as large as the size of the grid side (i.e., N_α) leads to poor results because Quickshift tends to segment the loss matrix into an insufficient number of regions. By fixing `kernel_size` and `max_dist` to $\sqrt{N_\alpha}$, we increase the segmentation density which is necessary to identify the best region in terms of task performance.

Grid density. We systematically test the robustness of Twin against different grid densities. We slice the log-spaced intervals of LR (α) and/or WD (λ) by sampling values every one, two, or three steps and refer to such operations with the python slicing notation `[::x]`. We average the error of Twin (FIFO scheduler) against the *Oracle* across 34 different configurations (as Fig. 3) and show the analysis in Tab. 4b. The MAE remains almost unaffected and close to 1.3% obtained with default settings to show Twin’s support to various grid intervals.

Dataset	Model	Optim. Setup	Performance	(M)AE
{C10, C100, ES, I2018, c10, CM}	{WRN-16-10, RN20, RN50}	SGD	75.0	1.8
		SGDM	75.6	1.2
C100	CVT-7/8	AdamW	68.8	0.0
C10	MLP-4-256	Adam	65.5	0.6
c10	WRN-16-10	Adam	54.5	0.6
C10	RN20	SGDM (piece-wise)	91.0	1.7
		SGDM (cosine)	90.5	2.2

Table 6: Ablation concerning the usage of different optimization setups. Performance is the (balanced) test accuracy. The (M)AE (\downarrow) is computed against the *Oracle* baseline.

Early stopping. In Tab. 5, we ablate concerning the impact of the early stopping scheduler. As visible, Twin effectively accommodates $HB_{25\%}$ or $HB_{12\%}$. Practitioners could safely default to either of the two, with $HB_{25\%}$ slightly ahead. The drop in performance for RNX_{101} with $HB_{12\%}$ is due to the small 7×7 grid employed. We refer to the Appendix for additional comments and guidance.

Optimizers and schedulers. In all experiments throughout the paper, we employed SGD with momentum (SGDM) and cosine scheduler as standard practice in deep learning. In this paragraph, we ablate on the possibility of using different optimization setups. In particular, we test plain SGD in six configurations involving RN20 on CIFAR-10/100, WRN-16-10 on ciFAIR-10, and RN50 on EusoSAT, ISIC 2018, and CLaMM. We also test RN20 with a piece-wise LR scheduler. Finally, we train ConvNets, MLPs, and transformers with either Adam [23] or AdamW [36], two popular choices when training such models. In Tab. 6, we notably observe that Twin also closely follows the *Oracle* in terms of (mean) absolute error (M)AE in such alternative optimization setups.

5 Conclusions

We introduced Twin, a simple yet effective HP tuning approach that reliably predicts learning rate and weight decay without using validation sets. Twin is not only beneficial in practice for simplifying model selection pipelines but also provides additional insights into the predictability of generalization for deep networks. Twin showed robust performance from a broad suite of experimental scenarios, including varying dataset sizes, imaging domains, architectures, model scales, and training setups. In this paper, we exclusively focused on image classification problems. However, future work could explore the application of Twin to computer vision tasks and beyond. Moreover, there is potential for extending Twin to alternative regularization strategies beyond L_2 penalty.

References

1. Barz, B., Denzler, J.: Deep learning on small datasets without pre-training using cosine loss. In: IEEE/CVF Winter Conference on Applications of Computer Vision

- (WACV) (2020) 3
2. Barz, B., Denzler, J.: Do we train on test data? purging CIFAR of near-duplicates. *Journal of Imaging* 6(6) (2020). <https://doi.org/10.3390/jimaging6060041>, <https://www.mdpi.com/2313-433X/6/6/41> 9
 3. Benton, G., Finzi, M., Izmailov, P., Wilson, A.G.: Learning invariances in neural networks from training data. *Advances in neural information processing systems* (2020) 3
 4. Brigato, L., Barz, B., Iocchi, L., Denzler, J.: Tune it or don't use it: Benchmarking data-efficient image classification. In: *Proceedings of the IEEE/CVF International Conference on Computer Vision*. pp. 1071–1080 (2021) 1
 5. Brigato, L., Barz, B., Iocchi, L., Denzler, J.: Image classification with small datasets: overview and benchmark. *IEEE Access* (2022) 1, 3, 9, 10
 6. Brigato, L., Iocchi, L.: A close look at deep learning with small data. In: *2020 25th International Conference on Pattern Recognition (ICPR)* (2021) 3
 7. Brigato, L., Mougiakakou, S.: No data augmentation? alternative regularizations for effective training on small datasets. In: *Proceedings of the IEEE/CVF International Conference on Computer Vision (ICCV) Workshops* (2023) 1
 8. Bruintjes, R.J., Lengyel, A., Rios, M.B., Kayhan, O.S., Zambrano, D., Tomen, N., van Gemert, J.: Vipriors 3: Visual inductive priors for data-efficient deep learning challenges. *arXiv preprint arXiv:2305.19688* (2023) 3
 9. Codella, N., Rotemberg, V., Tschandl, P., Celebi, M.E., Dusza, S., Gutman, D., Helba, B., Kalloo, A., Liopyris, K., Marchetti, M., et al.: Skin lesion analysis toward melanoma detection 2018: A challenge hosted by the international skin imaging collaboration (ISIC). *arXiv preprint arXiv:1902.03368* (2019) 9
 10. Cubuk, E.D., Zoph, B., Mane, D., Vasudevan, V., Le, Q.V.: Autoaugment: Learning augmentation strategies from data. In: *Proceedings of the IEEE/CVF Conference on Computer Vision and Pattern Recognition* (2019) 3
 11. Dosovitskiy, A., Beyer, L., Kolesnikov, A., Weissenborn, D., Zhai, X., Unterthiner, T., Dehghani, M., Minderer, M., Heigold, G., Gelly, S., et al.: An image is worth 16x16 words: Transformers for image recognition at scale. *arXiv preprint arXiv:2010.11929* (2020) 3
 12. Elsken, T., Metzen, J.H., Hutter, F.: Neural architecture search: A survey. *The Journal of Machine Learning Research* (2019) 3
 13. Golovin, D., Solnik, B., Moitra, S., Kochanski, G., Karro, J.E., Sculley, D. (eds.): *Google Vizier: A Service for Black-Box Optimization* (2017) 6
 14. Goyal, P., Dollár, P., Girshick, R., Noordhuis, P., Wesolowski, L., Kyrola, A., Tulloch, A., Jia, Y., He, K.: Accurate, large minibatch sgd: Training imagenet in 1 hour. *arXiv preprint arXiv:1706.02677* (2017) 3
 15. Hassani, A., Walton, S., Shah, N., Abuduweili, A., Li, J., Shi, H.: Escaping the big data paradigm with compact transformers. *arXiv preprint arXiv:2104.05704* (2021) 12
 16. He, K., Zhang, X., Ren, S., Sun, J.: Deep residual learning for image recognition. In: *IEEE Conference on Computer Vision and Pattern Recognition (CVPR)* (2016) 3, 11, 12
 17. He, T., Zhang, Z., Zhang, H., Zhang, Z., Xie, J., Li, M.: Bag of tricks for image classification with convolutional neural networks. In: *Proceedings of the IEEE/CVF conference on computer vision and pattern recognition* (2019) 1
 18. Helber, P., Bischke, B., Dengel, A., Borth, D.: EuroSAT: A novel dataset and deep learning benchmark for land use and land cover classification. *IEEE Journal of Selected Topics in Applied Earth Observations and Remote Sensing* 12(7), 2217–2226 (2019). <https://doi.org/10.1109/JSTARS.2019.2918242> 9

19. Hendrycks, D., Dietterich, T.G.: Benchmarking neural network robustness to common corruptions and perturbations. In: 7th International Conference on Learning Representations, ICLR 2019, New Orleans, LA, USA, May 6-9, 2019 (2019) [4](#)
20. Heo, B., Chun, S., Oh, S.J., Han, D., Yun, S., Kim, G., Uh, Y., Ha, J.W.: Adamp: Slowing down the slowdown for momentum optimizers on scale-invariant weights. arXiv preprint arXiv:2006.08217 (2020) [3](#)
21. Immer, A., van der Ouderaa, T., Rätsch, G., Fortuin, V., van der Wilk, M.: Invariance learning in deep neural networks with differentiable laplace approximations. Advances in Neural Information Processing Systems (2022) [3](#)
22. Keskar, N.S., Mudigere, D., Nocedal, J., Smelyanskiy, M., Tang, P.T.P.: On large-batch training for deep learning: Generalization gap and sharp minima. arXiv preprint arXiv:1609.04836 (2016) [3](#)
23. Kingma, D.P., Ba, J.: Adam: A method for stochastic optimization. arXiv preprint arXiv:1412.6980 (2014) [14](#)
24. Kornblith, S., Shlens, J., Le, Q.V.: Do better imagenet models transfer better? In: Proceedings of the IEEE/CVF Conference on Computer Vision and Pattern Recognition. pp. 2661–2671 (2019) [3](#)
25. Krizhevsky, A.: Learning multiple layers of features from tiny images (2009) [12](#)
26. Krizhevsky, A., Sutskever, I., Hinton, G.E.: Imagenet classification with deep convolutional neural networks. Advances in neural information processing systems **25** (2012) [1](#), [2](#)
27. Le, Y., Yang, X.: Tiny imagenet visual recognition challenge. CS 231N (2015) [12](#)
28. Lengyel, A., Bruintjes, R.J., Rios, M.B., Kayhan, O.S., Zambrano, D., Tomen, N., van Gemert, J.: Vipriors 2: visual inductive priors for data-efficient deep learning challenges. arXiv preprint arXiv:2201.08625 (2022) [3](#)
29. Li, L., Jamieson, K., Rostamizadeh, A., Gonina, E., Ben-tzur, J., Hardt, M., Recht, B., Talwalkar, A.: A system for massively parallel hyperparameter tuning. Conference of Machine Learning and Systems (2020) [3](#), [6](#)
30. Li, L., Jamieson, K., DeSalvo, G., Rostamizadeh, A., Talwalkar, A.: Hyperband: A novel bandit-based approach to hyperparameter optimization. The journal of machine learning research (2017) [3](#), [6](#)
31. Li, Y., Hu, G., Wang, Y., Hospedales, T., Robertson, N.M., Yang, Y.: Dada: Differentiable automatic data augmentation. arXiv preprint arXiv:2003.03780 (2020) [3](#)
32. Li, Y., Wei, C., Ma, T.: Towards explaining the regularization effect of initial large learning rate in training neural networks. Advances in Neural Information Processing Systems (2019) [3](#)
33. Liu, Z., Kitouni, O., Nolte, N.S., Michaud, E., Tegmark, M., Williams, M.: Towards understanding grokking: An effective theory of representation learning. Advances in Neural Information Processing Systems **35**, 34651–34663 (2022) [2](#), [4](#), [5](#)
34. Liu, Z., Michaud, E.J., Tegmark, M.: Omnigrok: Grokking beyond algorithmic data. In: The Eleventh International Conference on Learning Representations, ICLR 2023 (2023) [5](#)
35. Lorraine, J., Vicol, P., Duvenaud, D.: Optimizing millions of hyperparameters by implicit differentiation. In: International conference on artificial intelligence and statistics (2020) [1](#), [3](#)
36. Loshchilov, I., Hutter, F.: Decoupled weight decay regularization. arXiv preprint arXiv:1711.05101 (2017) [14](#)
37. McMahan, B., Moore, E., Ramage, D., Hampson, S., y Arcas, B.A.: Communication-efficient learning of deep networks from decentralized data. In: Artificial intelligence and statistics (2017) [1](#)

38. Mlodozienec, B., Reisser, M., Louizos, C.: Hyperparameter optimization through neural network partitioning. arXiv preprint arXiv:2304.14766 (2023) [3](#)
39. Neelakantan, A., Vilnis, L., Le, Q.V., Sutskever, I., Kaiser, L., Kurach, K., Martens, J.: Adding gradient noise improves learning for very deep networks. arXiv preprint arXiv:1511.06807 (2015) [3](#)
40. Nilsback, M.E., Zisserman, A.: Automated flower classification over a large number of classes. In: 2008 Sixth Indian conference on computer vision, graphics & image processing. IEEE (2008) [9](#)
41. Power, A., Burda, Y., Edwards, H., Babuschkin, I., Misra, V.: Grokking: Generalization beyond overfitting on small algorithmic datasets. arXiv preprint arXiv:2201.02177 (2022) [4](#)
42. Russakovsky, O., Deng, J., Su, H., Krause, J., Satheesh, S., Ma, S., Huang, Z., Karpathy, A., Khosla, A., Bernstein, M., et al.: Imagenet large scale visual recognition challenge. International Journal of Computer Vision (IJCV) **115**(3), 211–252 (2015) [3](#), [10](#)
43. Schwöbel, P., Jørgensen, M., Ober, S.W., Van Der Wilk, M.: Last layer marginal likelihood for invariance learning. In: International Conference on Artificial Intelligence and Statistics (2022) [3](#)
44. Stone, M.: Cross-validatory choice and assessment of statistical predictions. Journal of the royal statistical society: Series B (Methodological) (1974) [1](#)
45. Stutzmann, D.: Clustering of medieval scripts through computer image analysis: towards an evaluation protocol. Digital Medievalist **10** (2016) [9](#)
46. Tan, M., Le, Q.: Efficientnet: Rethinking model scaling for convolutional neural networks. In: International conference on machine learning (2019) [9](#)
47. Touvron, H., Cord, M., Douze, M., Massa, F., Sablayrolles, A., Jégou, H.: Training data-efficient image transformers & distillation through attention. In: International conference on machine learning (2021) [10](#)
48. Van Laarhoven, T.: L2 regularization versus batch and weight normalization. arXiv preprint arXiv:1706.05350 (2017) [3](#)
49. Vapnik, V.: Principles of risk minimization for learning theory. Advances in neural information processing systems (1991) [8](#)
50. Varoquaux, G., Cheplygina, V.: Machine learning for medical imaging: methodological failures and recommendations for the future. NPJ digital medicine (2022) [1](#)
51. Vedaldi, A., Soatto, S.: Quick shift and kernel methods for mode seeking. In: 10th European Conference on Computer Vision, Marseille, France, October 12-18, 2008, Proceedings, Part IV 10 (2008) [6](#)
52. Wad, T., Sun, Q., Pranata, S., Jayashree, K., Zhang, H.: Equivariance and invariance inductive bias for learning from insufficient data. In: Computer Vision—ECCV 2022: 17th European Conference, Tel Aviv, Israel, October 23–27, 2022, Proceedings, Part XI (2022) [4](#), [8](#)
53. Wah, C., Branson, S., Welinder, P., Perona, P., Belongie, S.: The Caltech-UCSD Birds-200-2011 Dataset. Tech. Rep. CNS-TR-2011-001, California Institute of Technology (2011) [9](#)
54. Weiss, K., Khoshgoftaar, T.M., Wang, D.: A survey of transfer learning. Journal of Big data **3**(1), 1–40 (2016) [3](#)
55. van der Wilk, M., Bauer, M., John, S., Hensman, J.: Learning invariances using the marginal likelihood. Advances in Neural Information Processing Systems (2018) [3](#)
56. Worrall, D.E., Garbin, S.J., Turmukhambetov, D., Brostow, G.J.: Harmonic networks: Deep translation and rotation equivariance. In: Proceedings of the IEEE Conference on Computer Vision and Pattern Recognition (2017) [3](#)

57. Xie, S., Girshick, R., Dollár, P., Tu, Z., He, K.: Aggregated residual transformations for deep neural networks. In: Proceedings of the IEEE conference on computer vision and pattern recognition (2017) [9](#), [12](#)
58. Yang, G., Hu, E., Babuschkin, I., Sidor, S., Liu, X., Farhi, D., Ryder, N., Pachocki, J., Chen, W., Gao, J.: Tuning large neural networks via zero-shot hyperparameter transfer. *Advances in Neural Information Processing Systems* **34**, 17084–17097 (2021) [3](#)
59. Yang, J., Shi, R., Wei, D., Liu, Z., Zhao, L., Ke, B., Pfister, H., Ni, B.: Medmnist v2—a large-scale lightweight benchmark for 2d and 3d biomedical image classification. *Scientific Data* (2023) [11](#)
60. Yu, T., Zhu, H.: Hyper-parameter optimization: A review of algorithms and applications. *arXiv preprint arXiv:2003.05689* (2020) [1](#), [3](#)
61. Yun, J., Kim, B., Kim, J.: Weight decay scheduling and knowledge distillation for active learning. In: *Computer Vision—ECCV 2020: 16th European Conference, Glasgow, UK, August 23–28, 2020, Proceedings, Part XXVI 16* (2020) [3](#)
62. Yun, J., Lee, J., Shon, H., Yi, E., Kim, S.H., Kim, J.: On the angular update and hyperparameter tuning of a scale-invariant network. In: *European Conference on Computer Vision* (2022) [3](#)
63. Zagoruyko, S., Komodakis, N.: Wide residual networks. In: Richard C. Wilson, E.R.H., Smith, W.A.P. (eds.) *British Machine Vision Conference (BMVC)*. pp. 87.1–87.12. BMVA Press (September 2016). <https://doi.org/10.5244/C.30.87> [12](#)
64. Zhang, G., Wang, C., Xu, B., Grosse, R.B.: Three mechanisms of weight decay regularization. In: *7th International Conference on Learning Representations, ICLR 2019, New Orleans, LA, USA, May 6-9, 2019* (2019) [3](#)